OBTAINING AN ELECTRON ENERGY-LOSS SPECTRA FINGERPRINT

FOR THE χ AND κ PHASES OF ALUMINUM OXIDE

by

Michael Tanner

Submitted to Brigham Young University in partial fulfillment

Of graduation requirements for University Honors

Department of Physics and Astronomy

October 2007

Advisor:  Richard Vanfleet                Honors Representative:  R. Steven Turley

Signature: _____        Signature: _____

BRIGHAM YOUNG UNIVERSITY


DEPARTMENT APPROVAL



of a senior thesis submitted by

Michael Tanner



This thesis has been reviewed by the research advisor, research coordinator, and department chair and has been found to be satisfactory.




_____
Date                                    Richard Vanfleet, Advisor


_____
Date                                    Eric Hintz, Research Coordinator


_____
Date                                    Ross L. Spencer, Chair

ABSTRACT


OBTAINING AN ELECTRON ENERGY-LOSS SPECTRA FINGERPRINT

FOR THE χ AND κ PHASES OF ALUMINUM OXIDE

Michael Tanner

Department of Physics and Astronomy

Bachelor of Science

The crystal structure of $Al_2O_3$ is found naturally in at least seven different atomic arrangements or phases.  By heating gibbsite, an aluminum hydroxide, to different temperatures, the χ, κ, and α phases were obtained.  The phase of each was confirmed by diffraction analysis. The samples were then investigated using electron energy-loss spectroscopy (EELS) in order to obtain an EELS spectra fingerprint for each phase.  An EELS fingerprint was obtained for each phase, allowing phase identification in nanometer scale regions that cannot be measured by other means.

ACKNOWLEDGMENTS

AUTHOR'S NOTE

In the event that an interested physicist would like to contact me concerning my research methods, I would gladly like to enter correspondence. I may be contacted at michaelstanner@gmail.com

# Contents

# List of Figures

# Chapter 1

# Introduction

## 1.1  Aluminum and Aluminum Oxide

Aluminum is the most abundant metal in the earth's crust, yet it is almost exclusively found in nature bonded to different elements and not to other aluminum atoms. Most of this aluminum comes in the form of minerals like bauxite, granite, and feldspar, as well as the precious gems ruby and sapphire. In most cases, including all of the above but feldspar, aluminum is present in the minerals as an oxide or hydroxide. Even in feldspar, which involves other elements in its chemical makeup, the aluminum atom is surrounded by oxygen atoms [1].

Elemental aluminum, when under conditions of standard temperature, pressure, and atmospheric levels of oxygen will rapidly oxidize, turning the outermost few layers of aluminum atoms into a layer of aluminum oxide ($Al_2O_3$) a few nanometers thick. This protective oxide layer is responsible for the stability of aluminum, protecting the metal from further corrosion. Combined with the fact that it is rather lightweight when compared with other metals, aluminum has found wide application in the industrial

world, from telescope mirrors and rockets to toys and utensils, being second only to iron in annual production among the metallic elements.

## 1.2   Phases of Aluminum Oxide

$Al_2O_3$ itself has been confirmed to have at least 7 different conformations or phases, consisting of the thermodynamically stable $\alpha$-$Al_2O_3$, commonly known as corundum or sapphire, and at least 6 transition phases of $Al_2O_3$, each having a unique crystal structure.  Since crystal structure affects the properties of materials, each phase may have unique properties, resulting in different applications in the industrial world.  For example, the reaction rate of explosives can be enhanced by the addition of aluminum crystals as a catalyst, where the enhancement of the reaction is directly related to the phase and thickness of the oxide layer coating the aluminum particles [5].

Studies by Gertsman and Kwok have shown evidence that when aluminum particles are exposed to atmospheric oxygen, the resulting $Al_2O_3$ may very well be a mixture of phases of the transition $Al_2O_3$ phases [5].  In the future it may be useful in some industrial applications to understand what phase or phases of $Al_2O_3$ have formed, so that this certain kind of aluminum and its oxide can either be used in its proper application or can be altered so it only contains the desired phase with its desired qualities.

## 1.3   The Problem of Investigation on a Nanometer Scale

With advances in nanotechnology towards the end of the twentieth century came a great interest in nanoparticles.  The same materials on the microscale were found to have different properties on the nanoscale.  For example, those phases of $Al_2O_3$ that were

formerly used in micropowder form as a catalyst for explosions, propellants, and pyrotechnics were found to be even more effective as nanopowders [5]. It is reasonable to predict a need for a process to identify and differentiate between these phases on a particle-by-particle basis, or in the nanoscale region.

Although the crystal structures of most of the transition phases of $Al_2O_3$ are still poorly understood, the phases can be differentiated through x-ray diffraction analysis. However, this method has its limits: there must be a large sample size in order to obtain reliable results, making it useless in examining single nanoparticles [6]. This also cannot be used in commonly encountered mixed media situations where multiple phases of $Al_2O_3$ may be in close proximity to each other. In this case, all of the phases will contribute to the diffraction pattern, yielding an ambiguous diffraction pattern that is an irresolvable superposition of the patterns of each phase. The results of mixed media analysis look like $Al_2O_3$, but they are not phase-specific.

A possible solution to both the problem of small sample size and mixed media is found in the technique of electron energy-loss spectroscopy, or EELS. Using EELS, a beam of electrons with a known, narrow range of kinetic energies are directed through a sample into a collector, where the energy lost by each exiting electron is measured. As can be seen by a glance at an EELS atlas, material studied by EELS analysis may have a unique EELS spectrum of number of electrons versus energy lost [8]. This unique spectrum could be used to identify unknown materials by comparing their EELS fingerprint with tabulated EELS tables.

Since the beam of electrons can be very narrow when using EELS, it can be used to analyze nanoparticles in situations where diffraction techniques fail. It also is a solution to the mixed media problem. Using appropriate sample preparation techniques, a mixed media sample can be polished down to a thin area involving only

the phase in question. This area can then be examined via EELS, such that only the phase in question contributes to the fingerprint [7].

This leaves only one question: Can EELS be used to distinguish between materials with the same chemical formula but slightly different crystal structure? On first glance, current authoritative EELS data suggest no, but this is only because of the nascent nature of EELS technology. Although first postulated in the 1944, EELS did not become a widespread experimental method until the 1980s and 1990s, following the improvement of technology associated with the electron microscope [10]. Current EELS atlases give a distinct spectrum for each element and many minerals, but they lack the resolution needed to see distinguishing features within each curve because such high-resolution EELS spectra did not become available until quite recently. For example, the entry in *EELS Atlas* for $\alpha$-$Al_2O_3$ shows the first peak as a simple hump [8]. Recent studies done by both Cullen and Larsson using higher resolution have shown that this first curve is in fact two distinct curves, a higher one followed by a lower one within the span of an electron volt [2] [9].

## 1.4   Direction from Initial Studies

Studies by Larsson, Zackrisson, Halvarsson, and Ruppi indicate a general shape difference between EELS spectra of the $\alpha$, $\gamma$, and $\kappa$ phases [9]. Cullen and Vanfleet carried out studies on a high-precision microscope with a resolution of 0.3 eV, illustrating significantly different features in the shapes of the $\alpha$ and $\gamma$ phase EELS spectra. Their study yielded two "EELS fingerprints" that could be used to distinguish between the $\alpha$ and $\gamma$ phases of $Al_2O_3$ [2].

The aim of this thesis is to expand the studies done by Cullen and Vanfleet to include two more of the transition phases of $Al_2O_3$: $\chi$ and $\kappa$.

# Chapter 2

# Methods

## 2.1   Sample Preparation

The different phases of $Al_2O_3$ can all be obtained by heating aluminum hydroxides, such as the gibbsite $(Al(OH)_3)$ used in this experiment, to different temperatures. Figure 2 illustrates the several reaction paths that can be taken when four of the aluminum hydroxides, namely gibbsite, boehmite, bayerite, and diaspore, are heated from 100 °C to 1200 °C.  In this experiment, the uppermost path was followed, where gibbsite undergoes a transformation to first χ-, then κ-, and finally α-$Al_2O_3$ to obtain these phases for study.

Powdered microscale grains of gibbsite was obtained from Nabaltec [11] and annealed in a ceramic crucible in a Lab-Line (CTF 12/75/700) Tube Furnace.   To obtain the χ, κ, and α phases, gibbsite was heated in air to 500, 900, and 1185 °C respectively and held at each respective temperature for 24 hours prior to cooling in air to room temperature.

The cooled powder samples are then applied to a small copper mesh grid with a lacey carbon grid covering it, as shown in Figure 2.  The phases were placed in plastic
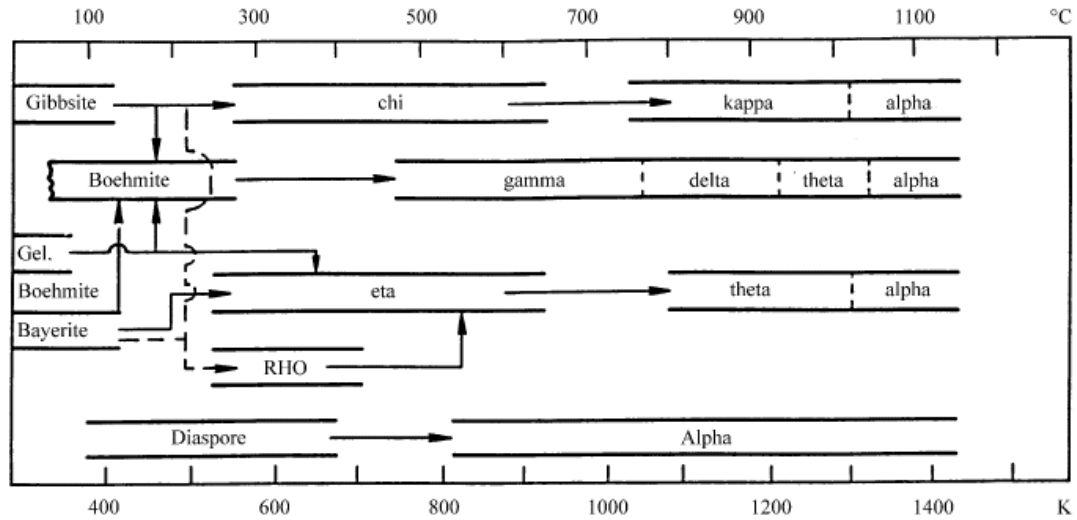
**Figure 1: Thermal Transformation Sequence of the Aluminum Hydroxides [6]**

The aluminum hydroxides are the leftmost entries in each row of the figure. When heated, the aluminum hydroxides will convert to a phase of aluminum hydroxide. Full conversion will take place after extended heating. The sample is held at the conversion temperature at 24 hours in this experiment. Conversion only proceeds appreciably from left to right. Although this figure shows that certain of the aluminum hydroxides can interconvert before the conversion to $Al_2O_3$ (indicated by vertical motion on the figure), this conversion is much smaller than the horizontal conversion [3], and has been considered negligible for this experiment.
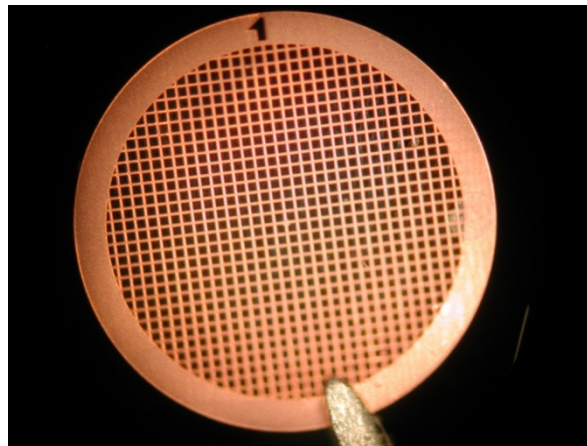


**Figure 2: Lacey Carbon Grid on Copper Mesh Grid**

A lacey carbon grid, invisible to the unaided eye, covers this copper mesh grid. The copper mesh grid has an actual diameter is 3 mm.

bags, followed by the copper grid. It was covered in the powdered phase and then removed. Although not visible to the unaided eye, microscale particles of $Al_2O_3$ had stuck to the lacey carbon grid, as seen in Figure 3.
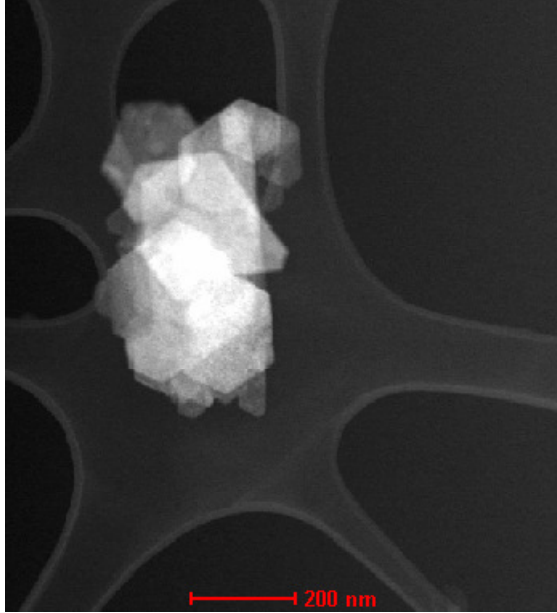
**Figure 3: STEM Image of $Al_2O_3$ Particles on Lacey Carbon Grid**

## 2.2   Phase Confirmation via Diffraction Analysis

To ensure accuracy in the results, the different phase samples were analyzed via diffraction analysis to confirm that each was in the desired phase of $Al_2O_3$. In this way the observed EELS spectra can be positively identified with a known phase.

On the molecular level $Al_2O_3$ has a regular crystal structure. Aluminum and oxygen atoms occupy spots in the crystal lattice in a distinct pattern for each particular phase of $Al_2O_3$. Because of this regular arrangement, a sheet of $Al_2O_3$ acts like a diffraction grating and will diffract both photons and electrons as they bend around the atoms, as is described in introductory physics textbooks.

This property is useful to us, as the locations of diffraction maxima are due to the regular atomic spacing in the lattice. The distance of diffraction maxima from the central maximum can measured to extract the distance between atoms in the original crystal lattice, commonly known as the d-spacings.
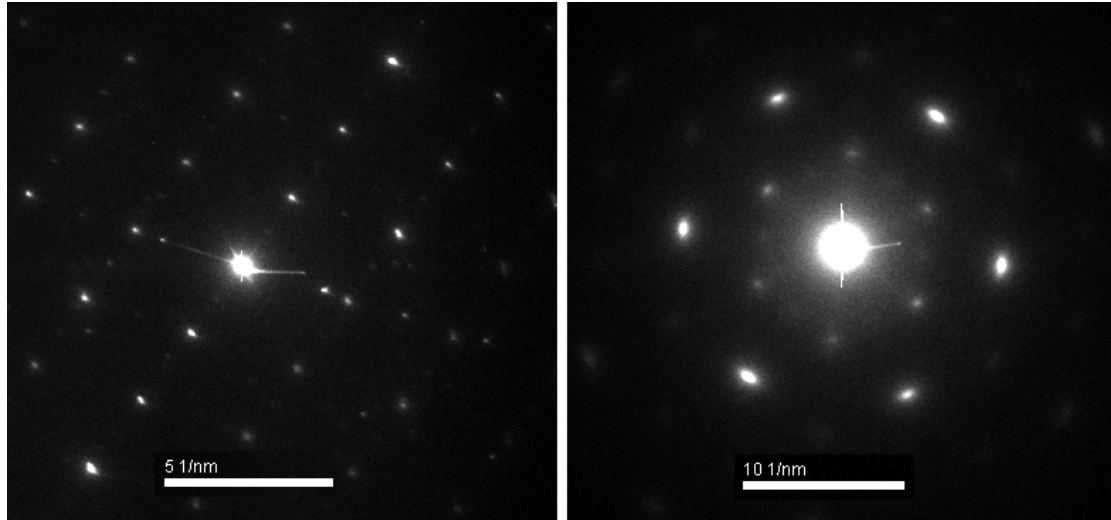
**Figure 4: Two Electron Diffraction Patterns from Gibbsite**

In these two patterns, the white spots designate diffraction maxima, with the bright center spot being the central diffraction maxima. These two very different spectra come from the same sample. Since sample orientation dictates the way that the electrons will diffract through the sample, several patterns are taken in order to capture all of the diffraction maxima.

These calculations for d-spacings are done using Bragg's law, which is

$$m \lambda = 2 d \sin(\theta)$$

(2.1)

where

λ is the wavelength,
d is the spacing between planes in the crystal,
θ is the angle of diffraction
and m is the order of the diffracted beam, an integer.

In this experiment the way electrons diffract through crystals is being studied, so the equation will be modified to fit this situation. In this case, since θ is small, we can use the small-angle approximation and replace $\sin(\theta)$ with $\tan(\theta)$. As is shown in Figure 5, $\tan(\theta)$ is equal to R/(2L), with R the distance from the central maxima and L the length to the screen, in this case the camera length.

Moving (2L) to the left-hand side and simplifying, we obtain

$$m \lambda L = d R$$

(2.2)

Since we are actually interested in the spacing between the peaks, m is replaced
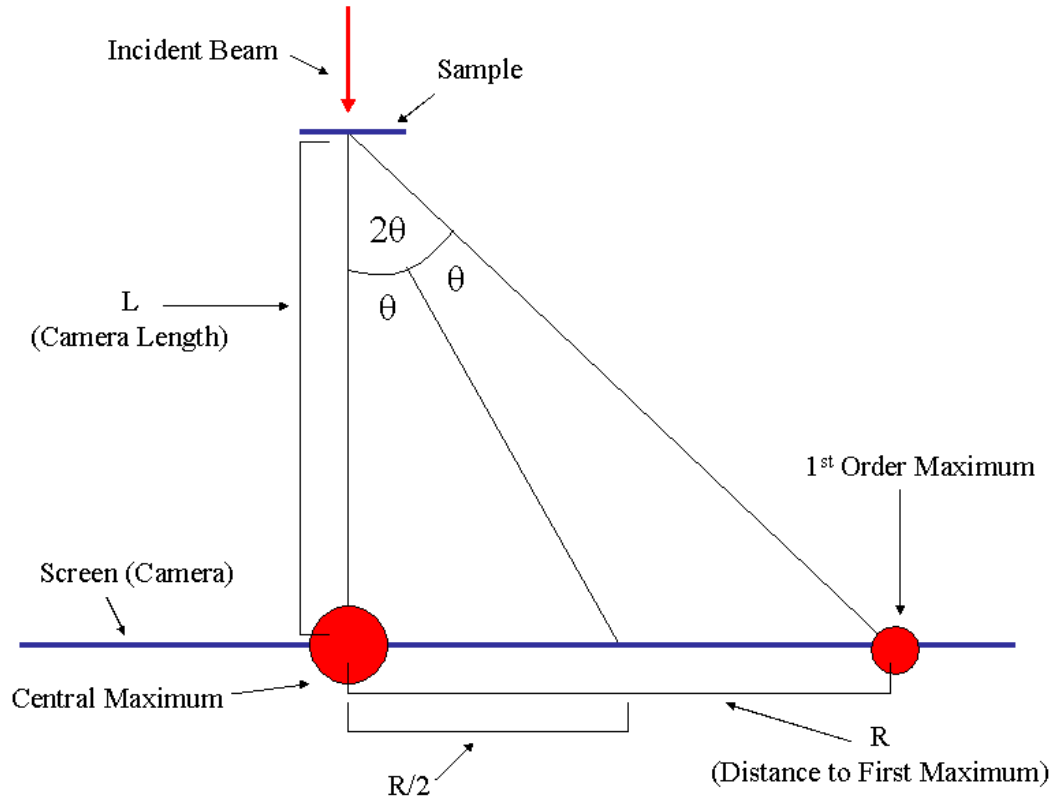
**Figure 5: Electron Diffraction Diagram**

with $\Delta m$ and set to 1 for our case.  Solving for the d-spacing d, we obtain

$$d = \frac{\lambda\, L}{R}$$

(2.3)

Once the d-spacing are obtained through this formula, they can be compared to tabulated data of the d-spacings for that certain material.  A good fit of the experimental data to the tabulated data is evidence that the material being analyzed is actually the material that it is expected to be.

Tabulated data exists for most of the phases of $Al_2O_3$ detailing the d-spacings in their crystal lattice.  One such table can be found in the appendix as reproduced in [4].  Using this table, the identity of a certain phase of $Al_2O_3$ can be confirmed by collecting electron diffraction data and then comparing calculated d-spacing with tabulated values.  In addition to spacing, this information can also involve the angle at which each

maximum occurred for the pattern.

Using Brigham Young University's Tecnai F20 Analytical STEM, many electron diffraction patterns were obtained for each sample. From these patterns the d-spacings in the crystal structures were measured. The d-spacings were then compared against the accepted x-ray diffraction values as located in the appendix, which in theory should be exactly the same as those obtained from electron diffraction. A great degree of similarity between experimental data and the tabulated data will allow for positive phase identification. Results from this phase of the experiment are discussed in later chapters.

## 2.3  EELS Spectra

Once confirmed to be each respective phase, a reliable EELS investigation of each phase can be conducted. In EELS, the energy lost by electrons as they pass through the sample is recorded. After microscope calibration, a beam of high-energy electrons is shot from an electron gun through a sample and into a collector under high vacuum. As the electrons pass through the sample, a number of things can happen to them. Referring to Figure 6 (following the electron paths from left to right), during its descent the electron can:

1. Pass straight through the sample without losing any energy and without any change in its direction. These electrons make up the zero-loss peak.

2. Lose a small amount of energy from electromagnetic interactions with other electrons and the nucleus, also possibly changing its direction. This is responsible for the plasmon effect, discussed below.

3. Be deflected by the nucleus and almost certainly not enter the collector, which is at the bottom of the figure.

4. Have an inelastic collision with core electrons in the sample, the incident electron losing a specific amount of energy corresponding to the increase in the core electron's energy. The incident electron's direction may also be changed. It then

passes into the collector.

5. (not pictured) Have an elastic collision with electrons in the sample, the electron keeping all of its energy but having its direction diverted. This is the interaction responsible for diffraction.

6. (not pictured) Experience any of the above in addition to number 2.
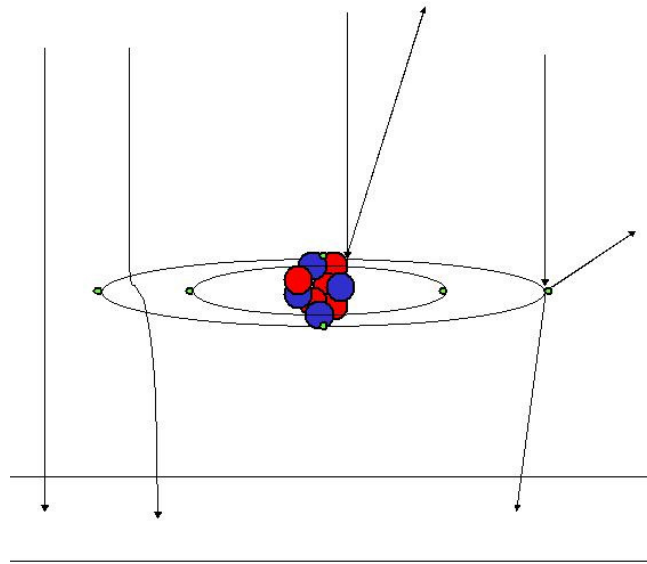


**Figure 6: EELS Diagram**

In practice, all samples are more than one atom thick, so often an electron may experience the above events many times. Due to these interactions, not all of the electrons that were initially put through the sample arrive at the collector because of a change in their direction, as the collector's aperture only has a diameter of 1-5 mm.

Those electrons that do make it to the collector are measured for their amount of energy loss. From this resulting data, an EELS spectrum can be created by plotting the amount of energy lost versus the number of collected electrons that lost that amount of energy.

There are many things to consider when obtaining EELS spectra. First, the level of resolution in an image will dictate the ability to distinguish between fine details in each spectrum. A convention for measuring this resolution is to measure the

full-width half-maximum (FWHM) value of the zero-loss peak (ZLP).  The ZLP

consists of those electrons that went through the sample but did not interact with it.

Before the electrons approach the sample, they pass through a monochromator that only

allows electrons with a certain amount of energy to pass and continue through to the

sample.

After these electrons pass through the sample without interacting with it, they

are collected and examined for how much energy they have, the energy value of the

peak of this narrow band being used as the standard against which the other electrons

are measured, now being defined as the point of zero energy loss.  The FWHM of this

spread is taken to be the resolution of the beam, and gives an indication of the amount

of detail that will be visible in the spectrum.

Higher resolution allows more details to be examined in each spectrum.  For

example, a glance at the entry for α-$Al_2O_3$ in the 1983 publication *EELS Atlas* [8]

shows a single peak at 78 eV.  This data was taken with a resolution of about 1 eV.

More recently, when two independent teams of scientists examined this same peak with

resolution ranging from 0.3 eV to 0.66 eV, this peak was shown to actually be two

peaks with slightly different heights [2][9].

One method for exercising slight control over the resolution is to change the

size of the entrance aperture to the collector.  Narrowing the aperture will decrease the

inherent angular spread of the beam and hence increase the resolution.  However, in

narrowing the aperture, the total number of electrons collected also decreases.  A lower

total count of electrons is a problem in obtaining a reliable EELS spectrum.  Each EELS

measurement has an inherent amount of noise with it, amounting to plus or minus a few

hundred counts of electrons.  Because of this noise, a large number of counts of

electrons originating from the electron gun must be registered by the collector in order

**The Zero-Loss Peak**
**7.18.07**



**The Zero-Loss Peak**
**Zoomed to the FWHM Region**
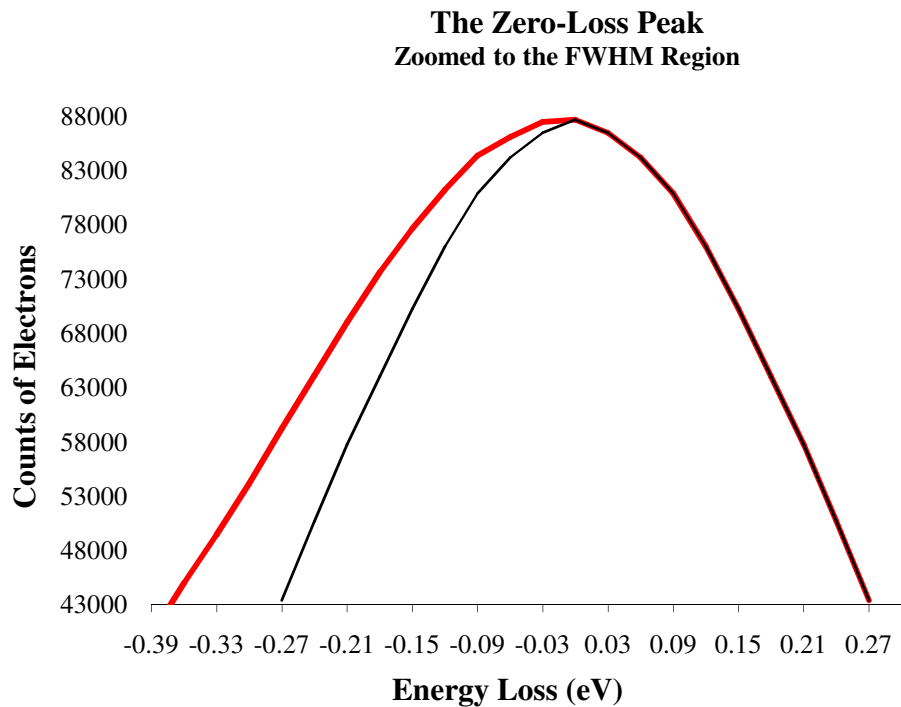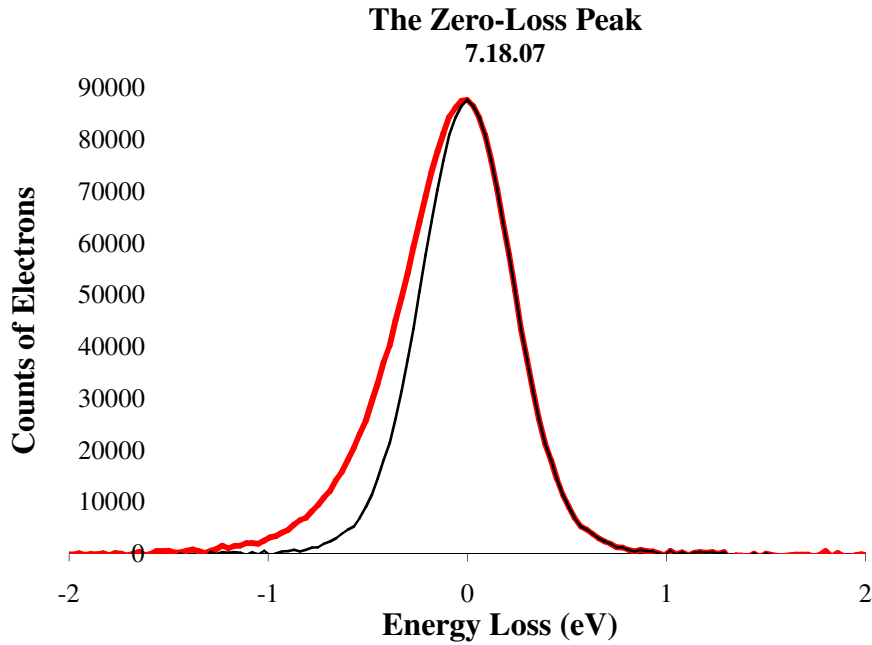


The ZLP is imaged in the above graphs, with the lower graph showing the span of the curves as they travel from their maximum in the middle to half of their height.  A typical narrow band of ranges of electron energies is shown by the black line displaying a Gaussian distribution of energies.  The red line shows a distorted ZLP obtained due to technical difficulties that are further discussed in Chapter 5.  This red ZLP is the one used for EELS in this experiment.  As is easily evident in the lower graph of the figure, the equipment malfunction caused a decrease in resolution as the FWHM increased from about 0.54 eV for the black curve to about 0.63 eV in the red curve.

to let the EELS spectrum details stand out from the inevitable noise. This can partially be accomplished by widening the entrance aperture. Hence, the entrance aperture size must be balanced in order to obtain maximum resolution.

In this study, 5 mm was the chief aperture size used, giving an average FWHM resolution of 0.63 eV. Aperture sizes of 2.5 mm and 1 mm were available, but this caused problems when trying to allow the spectrum to stand out from the noise. Greater resolution could be obtained through fine-tuning the monochromator settings, but the current level of resolution sufficed for the current experiment.

As previously mentioned, enough counts must be registered in the collector so that the spectrum stands out from the noise. In addition to widening the aperture, the spectrum can be made to better stand out from the noise by practicing EELS on the thinnest possible part of the sample. The thicker the sample, the less chance an electron has of reaching the collector after collision with atomic nuclei. Thus, if a thin sample is used, a higher resolution is allowed as the spectrum more easily stands out above the noise.

Once considerations to maximize resolution are made, an EELS spectrum can be obtained. A sample EELS spectrum is given below in Figure 8. The top figure is the original spectrum, showing the number of electrons counted between the loss levels of about 30 and 90 eV, as visualized by the black line. The aluminum edge of the spectrum is located at about 70 eV on this figure. Leading up to that area of the graph is a broad area of exponential decay from plasmon losses, a wide peak in energy loss on the spectrum that is chiefly due to the $2^{nd}$ factor in EELS spectra as listed above. These plasmon losses arise from both the carbon film and the $Al_2O_3$ crystal. The aluminum core lies on the tail of this plasmon peak.

In order to visualize only those electrons from the aluminum edge, a

background subtraction of the plasmon tail is made, which is visualized as the red line and is an extrapolation of the decaying plasmon. This is displayed in both the top and middle spectrum, which displays the same data as the top spectrum but is focused on the aluminum edge. The background is then subtracted from the original spectrum, and is indicated on the graphs as the blue line. The bottom spectrum is zoomed to the background-subtracted EELS spectrum of $\alpha$-$Al_2O_3$.

The original presence of the plasmon peak at the aluminum edge adds a measure of uncertainty to the data, as although it can be reasonably fit to a curve and subtracted off, it still can obviously affect the data. The only partial remedy for this is to take the EELS spectrum on a part of the sample that is not directly positioned over the carbon film (removing the plasmon vibrations of the $Al_2O_3$ spectrum is impossible, and the peak must still be subtracted). For example, in Figure 4, it is apparent that the part of the $Al_2O_3$ chunk at the top of the image has no carbon directly behind it, being suspended over a hole in the lacey carbon grid. Doing EELS on this part of the sample would be ideal so as to minimize the amount of carbon influence on the EELS spectrum.

After background subtraction, the left over electron counts are mostly from electron-electron collisions, which are the counts in which we are interested. They have distinct peak values because of the limited number of transitions an electron is allowed to make from a bound to an empty electron state.

There were a few more conventions that were adopted as the spectra were taken. First, they were all taken in diffraction mode. In this mode, the electrons at the central maximum are those that have not had their paths bent by diffraction, so there is less likelihood of stray electrons being in this part of the beam and making it into the collector. Furthermore, in diffraction mode it is easy to tell if the sample is too thick to

**EELS Background Subtraction in α-Al₂O₃**
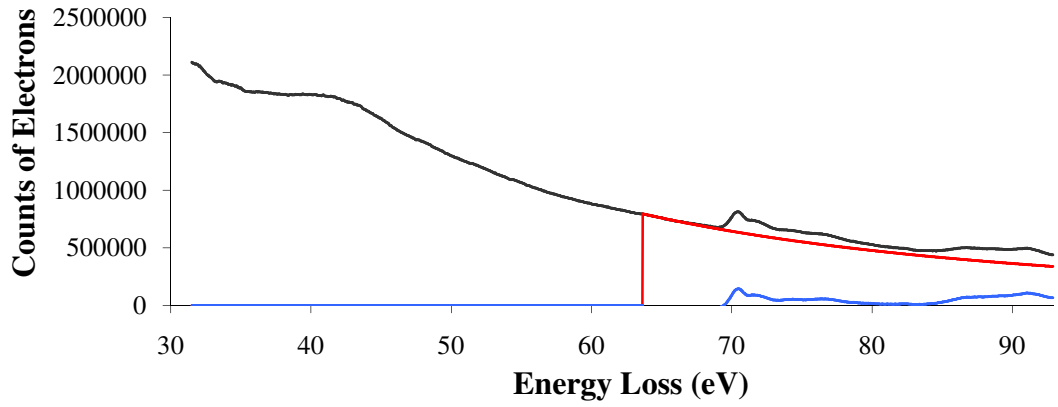


**EELS Background Subtraction in α-Al₂O₃**
**Zoomed to the Aluminum Edge**
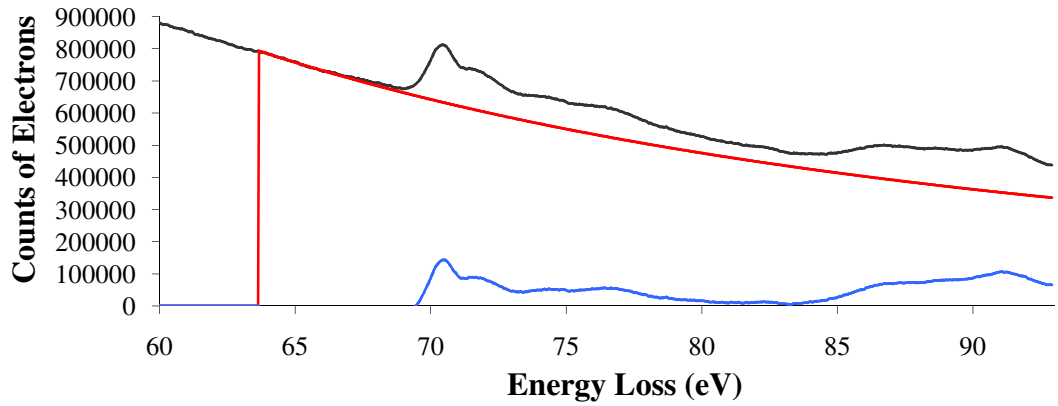


**EELS Background Subtraction in α-Al₂O₃**
**Zoomed to the Aluminum Edge, Background Subtracted**
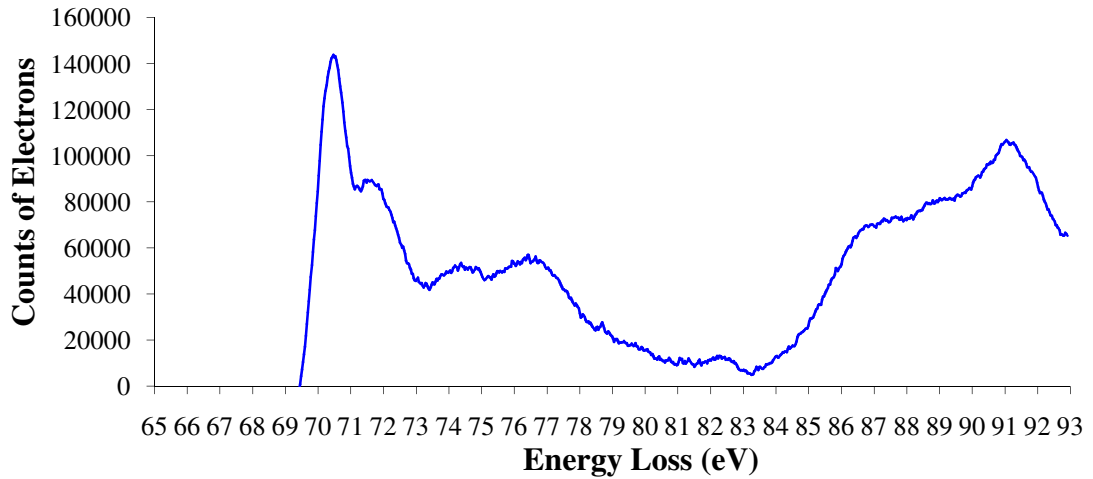
obtain a reliable EELS spectrum, as the distinction between the maxima and the spaces between them blur as the sample gets thicker due to the reasons discussed above.

Next, it was discovered that if a high-energy beam is left concentrated on a small part of the sample, it is not too long before it begins to damage and possibly cause phase change due to the transfer of energy from electrons to nuclei in collisions. Because of the great energy of the electrons coming through (200 k eV), if the beam is left at any place on the sample for too long, it will likely transfer enough energy to a very small part of the sample that it will undergo phase change into sapphire [5]. In fact, in the course of this investigation visible changes in the EELS spectrum were found after obtaining spectra from the same part of the sample over a period of leaving the beam on it, as recorded in Figure 9. This was avoided if at all possible.

The method employed to avoid this is first to find a suitable part of the sample, and then to increase the magnification to the limits of the TEM's ability (970,000x magnification) while focusing on a spot near but not on the part of the sample where the spectrum is to be taken. The sample is focused on and then put into diffraction mode. Since a fairly uniform part of the sample has been chosen, the focus of the image will not be distorted by minor spatial variations in the beam's location on the sample. Just as the spectrum is ready to be taken, the beam is moved to the imaging spot. The spectrum is immediately taken without further changing the focus, minimizing the amount of time the beam spends on the surface of the imaging area.

Since there can be great variation in the number of counts registered by the collector depending on the part of the sample being studied, after EELS spectra are collected, they are all scaled for easy comparison. After normalizing, the location on the spectrum with the highest count of electrons is now 1, with all other locations being specified as fractions of this maximum value.

Additionally, the eV scale on the horizontal axis may have an error of several eV, as the zero-loss peak tends to wander even within a few seconds of calibration. Since the aim of this study was to examine the shapes and features of the peaks, no special effort was made to continuously calibrate the energy scale for each spectrum.

For reference, the aluminum edge begins at about 78 eV, and in spectra comparisons the starting point of this edge is actually located at about this value and not at whatever is located on the x-axis, which is influenced by the wandering ZLP. Extra precautions to prevent the wandering of the ZLP were not considered.

**Figure 9: EELS Evidence of Sample Damage in κ-Al₂O₃**

**EELS Evidence of Sample Damage in κ-Al₂O₃**



**EELS Evidence of Sample Damage in κ-Al₂O₃**
**Zoomed to the First Peak Area**
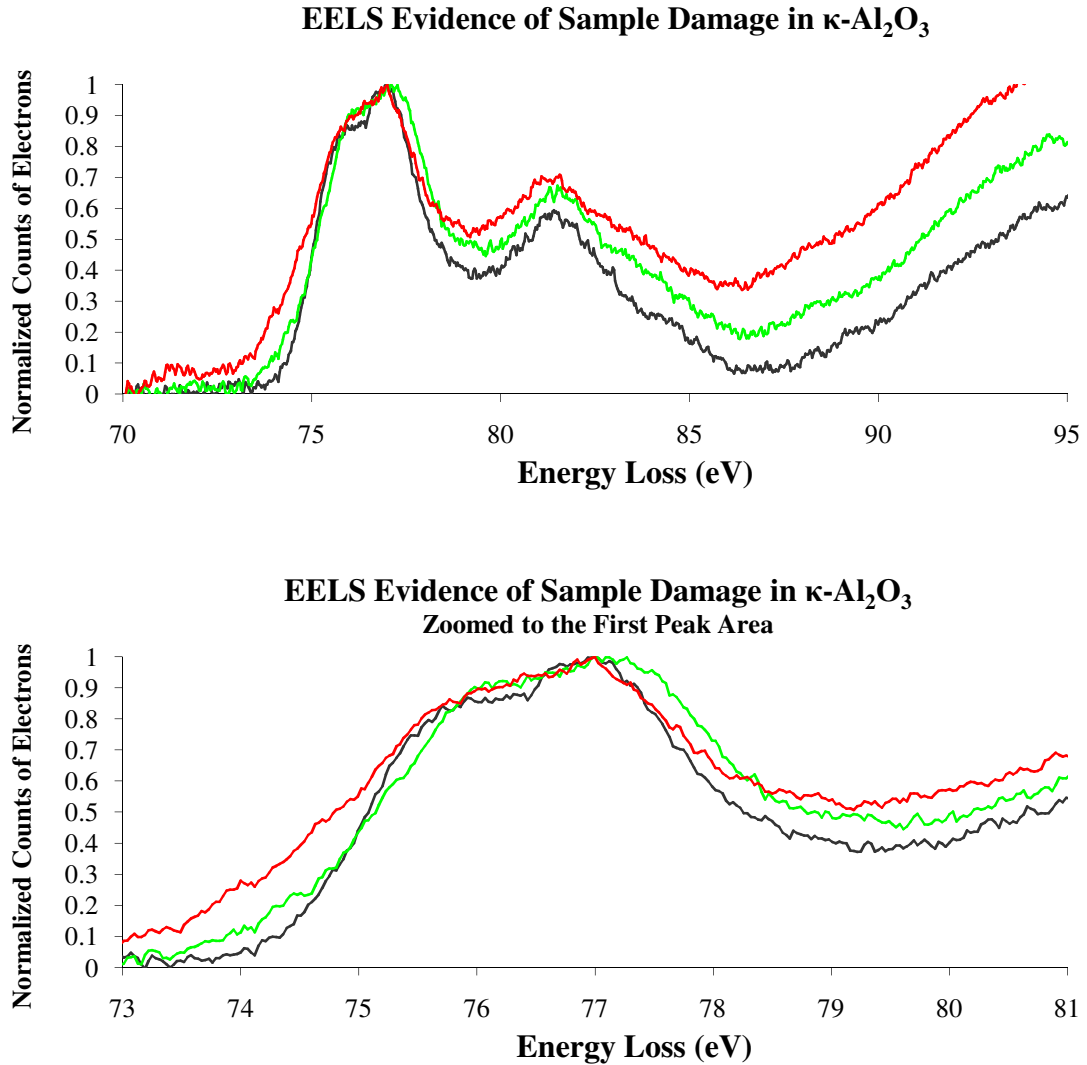


       The above 2 graphs illustrate sample damage in κ-Al₂O₃ from the electron beam over 2 minutes. The bottom graph is a section of the top graph, focused in to show the detail of the first two peaks. Immediately following calibration, the electron beam was moved to a nearby location on the sample and an EELS spectrum was obtained (black line).  The beam was left at this location, and 1 minute later another spectrum was taken (green line), followed by another spectrum taken 1 more minute later (red line).  As the time the beam is left on this location increases, the EELS spectrum becomes less distinct. The two peaks become harder to differentiate, and a general broadening of all peaks is observed.

# Chapter 3

# Experiment

## 3.1   α-Al$_2$O$_3$

The phase of Al$_2$O$_3$ which heretofore has received the most study is the α phase.

Having nearly identical EELS spectra recorded from several different sources of

contemporary research, it is not only a good starting point against which to compare the

data of the other phases, but by comparing my results with those of other researchers,

the accuracy of my results can be understood.

α-Al$_2$O$_3$ was prepared and analyzed according to the procedures stated in

Chapter 2.  Gibbsite was annealed in air at 1185 °C for 24 hours according to the recipe

in Table 1.

| Gibbsite to α-Al$_2$O$_3$ | | | | | |
|---|---|---|---|---|---|
| Step | 1 | 2 | 3 | 4 | 5 |
| Δ Temp (°C) | 600 | 100 | 50 | 25 | 25 |
| Temp (°C) | 900 | 1000 | 1100 | 1125 | 1185 |
| Dwell Time (h) | 0.1 | 0.1 | 0.1 | 0.1 | 24 |

**Table 1: Annealing Ramps and Temperatures for α-Al$_2$O$_3$**

In the table above, Δ Temp is the rate of heating in °C per hour, Temp is the temperature to which it is heated, and  Dwell Time is the time it is held at that temperature until proceeding to the next step.  After the final step, the furnace is shut off and the samples slowly cool to room temperature.

Electron diffraction spectra of α-Al$_2$O$_3$ were then obtained to confirm its phase.

Phase confirmation proved more difficult than originally postulated, and a great degree

of ambiguity still exists in the results of this phase of the experiment between the

phases.  This ambiguity is discussed in greater detail in Chapter 4.  The diffraction data

is included in Appendix B in an attached CD-ROM containing several pages of

diffraction data analysis, an explanation of which is also located in Appendix B.

α-Al$_2$O$_3$ was then examined using EELS as previously stated. Several spectra were obtained, all of which were very similar in appearance. A typical spectrum is shown below in Chart 1 with 0.63 eV resolution.

**Figure 10: α-Al$_2$O$_3$ EELS Spectrum**

**α-Al$_2$O$_3$ EELS Spectrum**
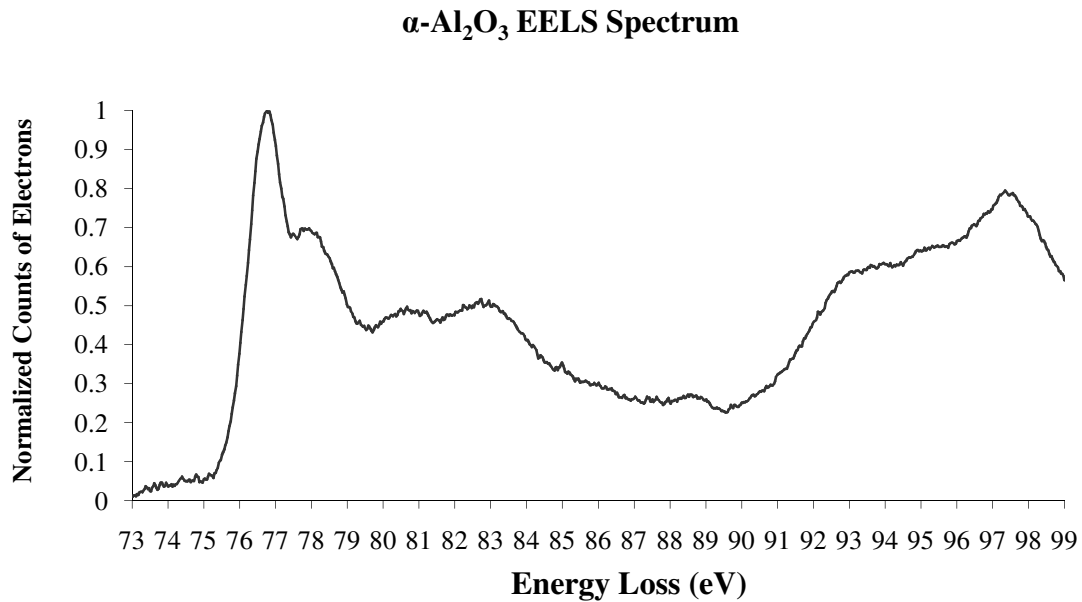


The aluminum edge reveals a pattern that in general features resembles those of Al$_2$O$_3$ in EELS atlases. The first two peaks centered around 77 eV are distinct, with the first peak being much more prominent than the second.

## 3.2   χ-Al$_2$O$_3$

Gibbsite was annealed in air at 500 °C for 24 hours according to the recipe in Table 2, yielding χ-Al$_2$O$_3$.

Diffraction analysis for χ-Al$_2$O$_3$ yielded results of similar quality to that of α-Al$_2$O$_3$, and is discussed further in the next chapter. It was then examined using EELS. Several similar spectra were obtained. A representative spectrum is shown below in Chart 2 with 0.63 eV resolution.

| Gibbsite to $\chi$-Al$_2$O$_3$ | | | | |
|---|---|---|---|---|
| Step | 1 | 2 | 3 | 4 |
| Δ Temp (°C) | 300 | 100 | 50 | 25 |
| Temp (°C) | 425 | 475 | 490 | 500 |
| Dwell Time (h) | 0.1 | 0.1 | 0.1 | 24 |

**Table 2: Annealing Ramps and Temperatures for $\chi$ -Al$_2$O$_3$**

Refer to Table 1 for explanatory notes.

**Figure 11: $\chi$-Al$_2$O$_3$ EELS Spectrum**

**$\chi$-Al$_2$O$_3$ EELS Spectrum**
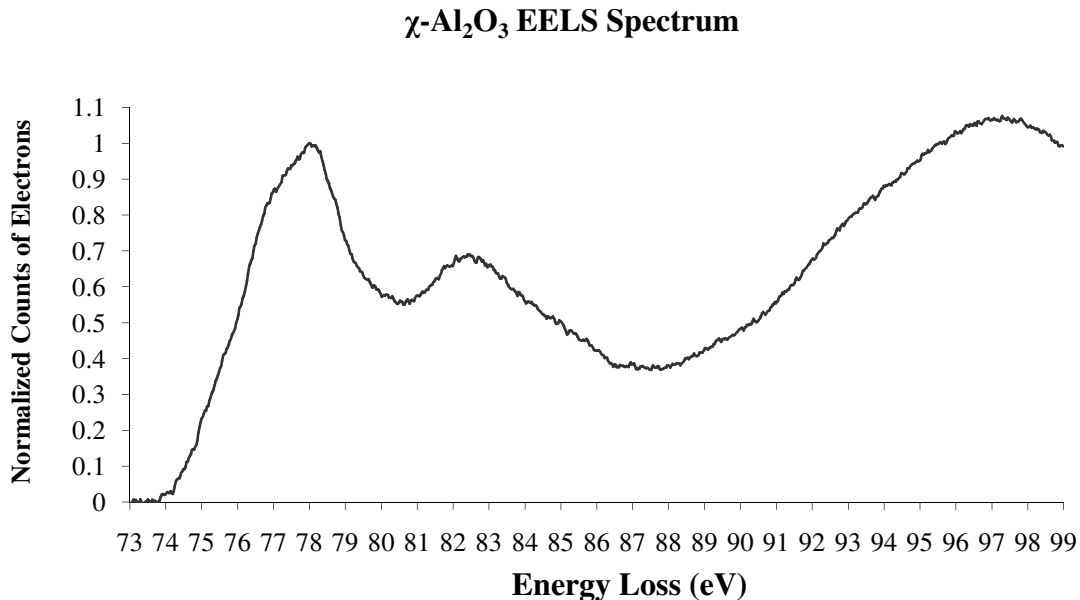


This spectrum, like the previous one, has the general shape of the Al$_2$O$_3$ spectrum, but the features seem to be broadened, with fewer distinguishable features. The area around 77 eV is not distinguishable as two separate peaks, but the peak does not have a simple Gaussian shape. The peak encounters points of abrupt change in slope at about 77 and 78 eV.

## 3.3  $\kappa$-Al$_2$O$_3$

Gibbsite was annealed in air at 900 °C for 24 hours according to the recipe in Table 3, yielding $\kappa$-Al$_2$O$_3$.

| Gibbsite to $\kappa$-Al$_2$O$_3$ | | | | |
|---|---|---|---|---|
| Step | 1 | 2 | 3 | 4 |
| $\Delta$ Temp (°C) | 800 | 100 | 50 | 25 |
| Temp (°C) | 800 | 850 | 875 | 900 |
| Dwell Time (h) | 0.1 | 0.1 | 0.1 | 24 |

**Table 3: Annealing Ramps and Temperatures for $\kappa$-Al$_2$O$_3$**

Refer to Table 1 for explanatory notes.

Diffraction analysis for $\kappa$-Al$_2$O$_3$ yielded results of similar quality to that of $\alpha$-Al$_2$O$_3$ and $\chi$-Al$_2$O$_3$, and is discussed further in the next chapter. It was then studied using EELS. Of the several similar spectra obtained, one representative spectrum is shown in Figure 12, having 0.63 eV resolution. In this spectrum the area around 77 eV is distinguished fairly well into two peaks, with the first peak being significantly lower than the second, unlike the $\alpha$ phase spectrum.

**Figure 12: $\kappa$-Al$_2$O$_3$ EELS Spectrum**

**$\kappa$-Al$_2$O$_3$ EELS Spectrum**
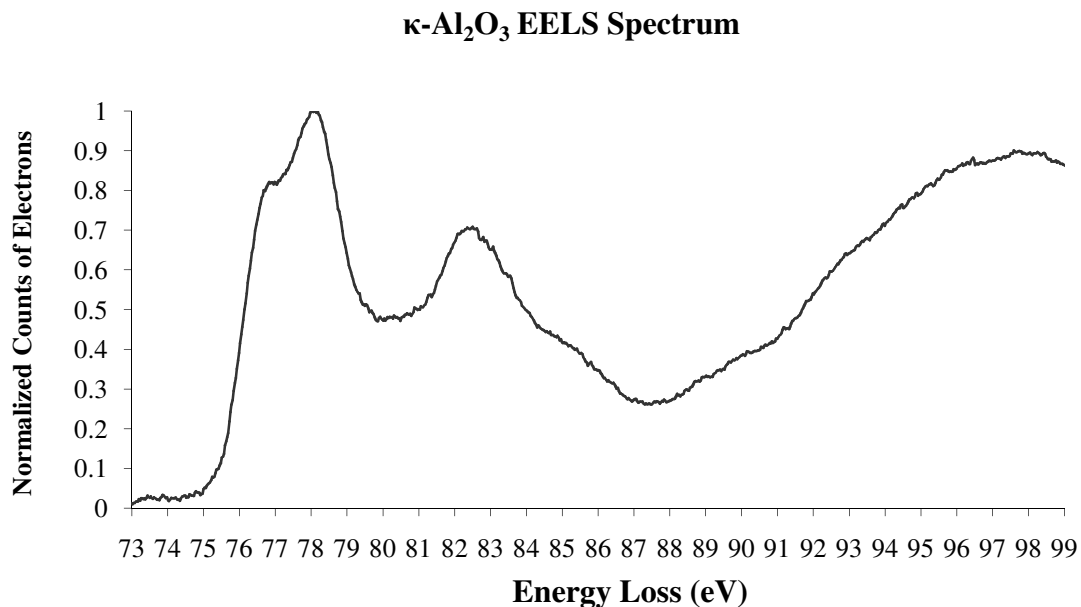
# Chapter 4

# Results and Analysis

## 4.1   α-Al$_2$O$_3$ Results Compared with Earlier Research

One important way that my research methods for all of the phases can be validated is by

agreement of the result of my methods with previous research.  This was my aim in

studying α-Al$_2$O$_3$.  The results of my spectra are plotted with those of two other

researchers in Figure 13.

There is a very close correlation between the contour of the spectrum at every

point of the graph between my spectra and the other two.  The most significant

difference occurs at the second peak, where the spectrum I obtained has a somewhat

more distinctive peak.  This suggests that my methods for obtaining EELS spectra are at

least as valid as those used by these researchers.

**Figure 13: α-Al₂O₃ EELS Spectra from Three Studies**
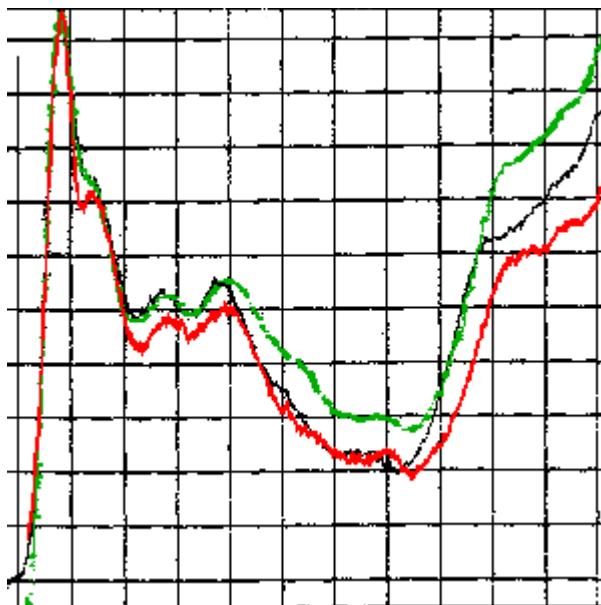


Data from this experiment is shown in red, that from [9] in green, and that from [2] in black, normalized to accommodate mutual plotting. The normalization process is discussed in section 4.2 in detail. All graphs were overlaid over the one with the least resolution, which is why there is a somewhat grainy appearance to this graph.

## 4.2   Phase-Comparative EELS Data

The EELS spectra of each studied phase are overlaid in Figure 14 for comparison and analysis. A rough general correlation can be seen in the peak shape trends for all of the phases. The 0.63 eV resolution definitely allows for examination of more subtle differences between the spectra that were impossible to distinguish in past years. I focus chiefly on the first two peaks, as all other subsequent peaks are affected by trailing plasmon effects from these peaks.

With the peak height normalized to the higher of the first two peaks for each spectrum, comparison is relatively simple. The first peak for the α phase occurs at about 77 eV and is defined as 100% of the peak height. This location corresponds to a shoulder with about 80% peak height in the κ phase. At the current resolution the χ phase at this location, however, is not a peak, but only a gentle slope up to the peak at

**Figure 14: Al$_2$O$_3$ Combined Phase EELS Spectra**

**Al$_2$O$_3$ Combined Phase EELS Spectra**
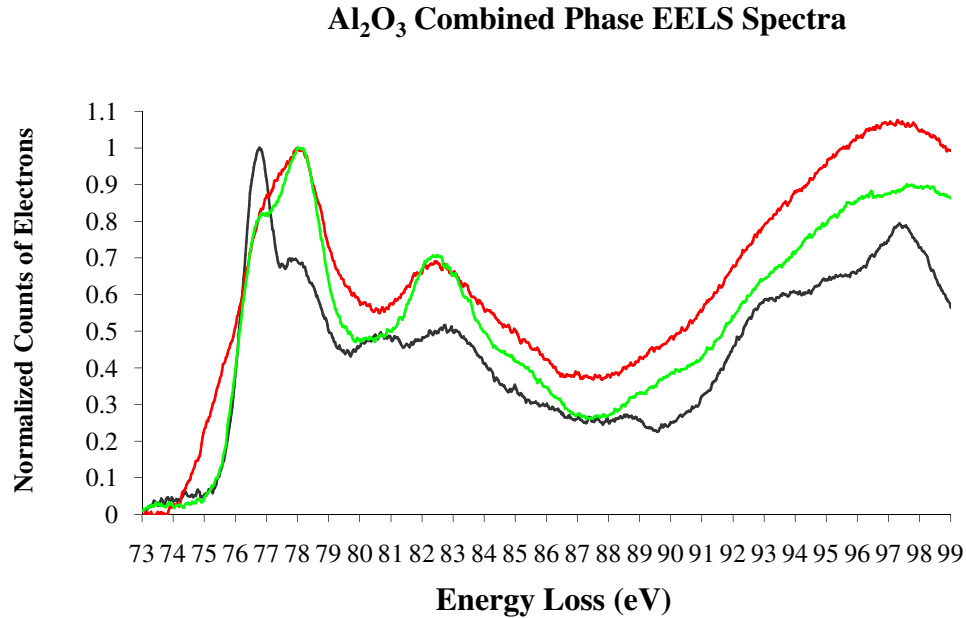


α-Al$_2$O$_3$ is in black, χ-Al$_2$O$_3$ is in red, and κ-Al$_2$O$_3$ is in green.

78 eV.  However, the spectrum appears to be undergoing a transition at the point of the first α peak, manifest as a decrease in slope.

The second peak contains more differences.  This is the peak that was defined to occur at 78 eV in each phase.  Despite this definition, the distance between this peak and the previous peak (or slope change in the case of χ-Al$_2$O$_3$) remains constant through all phases.  At this peak, the χ and κ phases attain their 100% maximum, and the α spectrum peak drops to about 70%.

## 4.3  Discussion of Experimental Error

Despite efforts to keep this scientific investigation free from errors, there are some known sources of error in this experiment.  First, the sample preparation process does have a source of error in the annealing times and temperatures.  The sources to which I had access for annealing the phases of Al$_2$O$_3$ from gibbsite were limited in that they did not suggest annealing times to ensure complete conversion of gibbsite or another phase

of $Al_2O_3$ to the phase in question, and they also specified a rather broad temperature range at which each phase occurred.

This left some doubt in my mind as to how much of my sample really was the phase in question, and how much consisted of leftover traces of other phases or gibbsite.  I chose a 24 hour annealing time to try to prevent this difficulty, but this determination was arbitrary at best.  My fears were also confirmed when I found a small spot in my $\alpha$-$Al_2O_3$ sample whose EELS spectra was unlike the rest of the sample and strongly resembled that of $\kappa$-$Al_2O_3$.  I then wondered if the same situation was present in my other samples in appreciable amounts.  Since an established EELS spectrum for the other phases in study is not currently extant, I would have problems distinguishing phases, especially if their spectra contain strong similarities.  Since there are also similarities between the electron diffraction patterns of these phases, and since only a certain percentage of the sample may not have transformed to the succeeding phase, it makes it more difficult to state with complete certainty the identity of the entire sample.

The difficulty I had in confirming the identity of each phase also shows that this error may have been significant.  In trying to pair up the experimentally obtained diffraction patterns with tabulated data there was ambiguity, as each of the studied phases fit several of the other phases' patterns, and had many additional diffraction spots that could not be explained by the tabulated data.  The fact that these phases still showed distinct EELS patterns is promising, but nevertheless cannot unequivocally be demonstrated by the results of this experiment.

This could possibly be due to inaccuracies in the diffraction data.  One problem that could have rendered this data inaccurate would be an improper calibration of the microscope in the taking of diffraction data.  Because the calibration we were looking at involved only the scaling factor of the diffraction patterns, the only obstacle to correct

data was finding a suitable constant by which to multiply the scaling factor. If the factor was the only inaccuracy, if the diffraction patterns could be set up to no longer depend on d-spacing but on a ratio of d-spacings compared to the largest d-spacing, the data would be accurate and could be compared to tabulated data that were likewise set up as ratios.

However, this did not work as well as imagined. Because each diffraction pattern is dependent on the orientation of the crystal that produced it, patterns possibly could lack the diffraction maxima corresponding to the largest d-spacing. Since we could not know whether this was true or not, we had no idea whether we were basing the d-spacing ratios on the largest d-spacing or the second, third, and so on largest d-spacing.

I began combating this problem by setting up d-spacing ratios based on many different d-spacing, but it quickly became apparent that this not only was inefficient but also inaccurate, because even if I found a d-spacing ratio that seemed to fit the corresponding ratio for the scheme of a particular phase of $Al_2O_3$, I had no way of confirming whether or not the ratio I had chosen was or was not chosen correctly.

We also sought to manage this problem by attempting to manually configure the data. Dr. Vanfleet suggested that we take diffraction data from a sample of known identity and compare it to tabulated data. By seeing the difference in this data and applying equation (2.3), we would able to come up with a correct scale factor for each camera length that would calibrate our data correctly. Thus we put a sample of silicon crystals into the TEM and analyzed its pattern as stated, coming up with the scale factors for several different camera lengths. Later I expanded this to use in odder camera lengths by fitting these points of camera length versus scale factor to a power law using Microsoft Excel 2007 and obtained the fit displayed in the figure below.

**Camera Length versus Scale Factor**
with Power Law Fit



$y = 6.350x^{-0.98}$
$R^2 = 0.999$

*Camera Length (mm)* — x-axis
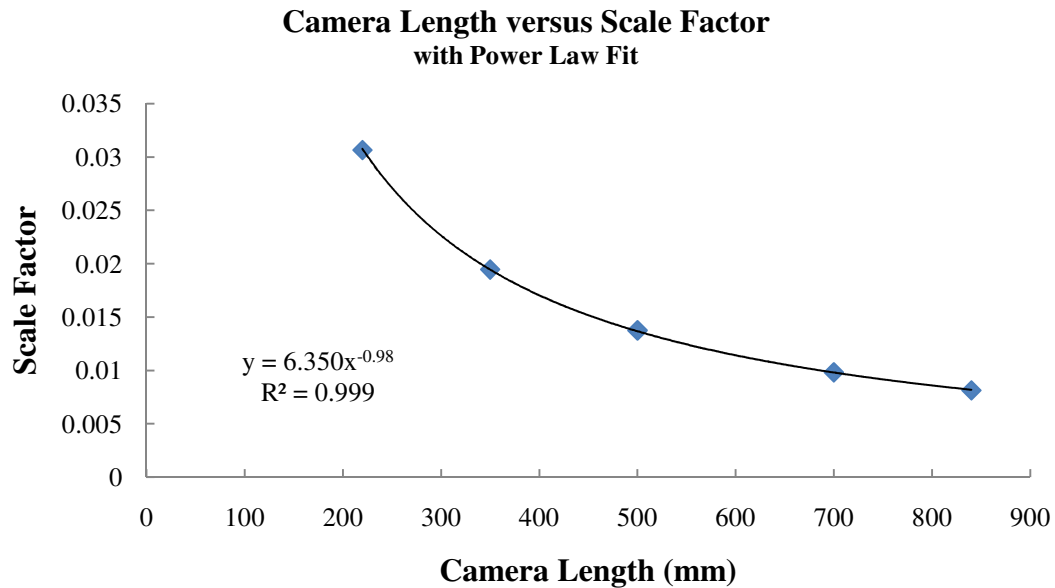
*Scale Factor* — y-axis

This scale factor was applied to the diffraction patterns, giving us theoretically accurate d-spacings for each phase, inasmuch as our calibration using the standard d-spacing values of Si was correct. Despite this apparent good fortune, the data still didn't seem to make sense. Almost every diffraction pattern seemed to lack the diffraction maxima corresponding to the largest d-spacings (which would explain why I had so much trouble in our first attempt to work out the calibration problem). There are a few possible explanations for this. First, those maxima corresponding to the largest d-spacing have the smallest distance from the central maximum, so these maxima may be indistinguishable from the central maximum due to its greater intensity and often spread out nature.

There is also a small amount of error in taking these patterns due to the nature of the material. Ideally, the diffraction patterns are caused by electrons undergoing a single diffracting event in the sample. With electrons, single events are uncommon, so my diffraction patterns likely contain maxima that are not in the tabulated data due to multiple diffraction events happening before the electrons leave the sample. I sought to minimize this problem by diffracting electrons through thinner areas of the sample, but

this source of error is not avoidable with electrons. Also, it seems very likely that there are more diffraction maxima resulting from single-crystal interactions than those listed in the table (see Appendix A), especially for those that only have a few entries, such as $\chi$-$Al_2O_3$ [7].

Possibly the most troublesome source of error in this experiment is in obtaining accurate EELS spectra. Due to equipment error late in the experiment which is discussed in detail in Chapter 5, the resolving power of the ZLP was reduced, changing from FWHM of 0.54 eV to 0.63 eV, as is visualized in Figure 7. Also, due to the wandering of the ZLP, by the time an EELS spectrum is taken, the results are often shifted off several eV from where they ought to be. I tried to remedy this by setting the second or only present peak in the EELS spectra to the 78 eV position, but this is assuming that this is the actual position of the peak. Although in my observations this is about the place where this peak lies, this shifting of the spectra clearly introduces errors when comparing to other shifted spectra. I suspect that this source of error was not too prominent, though, because the shape of the obtained spectra tends to follow the same shape at the same level of eV loss despite this shift. In future studies it would perhaps be prudent to realign the ZLP immediately before obtaining each spectrum; for the present, however, it has been deemed tedious, and hence introduces a small margin of error.

The possibility of sample damage and conversion to other phases of $Al_2O_3$ was discussed in Chapter 2. The procedure was planned to avoid this, so it is not believed to be a problem, though it is still a possible source of experimental error.

# Chapter 5

# Conclusion

## 5.1 Experimental Conclusions

In this experiment the goal was to obtain EELS fingerprints for $\chi$- and $\kappa$-$Al_2O_3$ and evaluate their utility for phase identification. The EELS spectra of these two phases are clearly distinct from $\alpha$-$Al_2O_3$ and each other. In the $\alpha$ phase the highest peak at the oxygen edge is the first peak, whereas in the $\kappa$ phase the second peak is the higher one. The $\chi$ phase seems only to have a single peak centered around the position of the second peak of the spectra of the other two phases, though a slight shoulder is evident at the position of the first peak in the other two phases. Furthermore, all of the peaks in this phase seem broader.

The most significant problem with these results, however, is that phase confirmation tests turned out poorly, so I cannot be sure that the samples are actually in the phase that I claim they're in. Future researchers should consider more accurate ways to characterize each phase.

## 5.2  Outlooks on Future Research

Results from this project naturally suggest EELS investigation into the remaining phases of $Al_2O_3$ for subtle differences in the peaks at the aluminum edge. This project had originally been scaled to study at least one other phase of $Al_2O_3$, but technical difficulties late in the project prevented the inclusion of data for other phases. Since the inception of this project, my skills in operating the TEM and interpreting the data obtained therefrom have continually improved; hence my micrographs and EELS spectra taken later in the project are significantly more authoritative than earlier ones. Unfortunately, in the spring and summer of 2007 the TEM could not be calibrated for EELS due to causes of idiopathic origin. This was a great hindrance in obtaining data, frustrating further study. In this section I present a few fragmentary results of my research for the benefit of future researchers, especially for those at BYU that may continue this project, including vital information for other samples that I made which they may use in their research.

First, for the benefit of other BYU researchers that may use my samples, the remaining samples not discussed in this paper are shown below in Table 4, complete with recipes of how they were annealed. Those samples obtained by annealing Catalpa A Boehmite took on a slight reddish color that was first recognized months after the annealing process, so an examination of the chemical composition of this phase would be encouraged, as it likely has some trace impurities that have caused the color change. No other data from examining these phases was deemed accurate enough to include. Another way this research could be extended is by gathering and comparing data from another part of the EELS spectrum, particularly the oxygen edge. The oxygen edge occurs at around 540 eV on the EELS spectrum, and corresponds to energy loss from interactions between electrons and oxygen in the sample. A preliminary investigation

of the oxygen edge of $\chi$- and $\kappa$-Al$_2$O$_3$ was made, the results of which are summarized in Figure 16.

**Table 4: Annealing Ramps and Temperatures for θ-, γ-, and δ-Al$_2$O$_3$**

| Boehmite (Catalpa A) to θ-Al$_2$O$_3$ | | | | | | |
|---|---|---|---|---|---|---|
| Step | 1 | 2 | 3 | 4 | 5 | 6 |
| Δ Temp (°C) | 600 | 100 | 100 | 50 | 25 | 25 |
| Temp (°C) | 800 | 875 | 925 | 960 | 980 | 990 |
| Dwell Time (h) | 0.1 | 0.1 | 0.1 | 0.1 | 0.1 | 24 |

| Boehmite (Catalpa A) to γ-Al$_2$O$_3$ | | | | |
|---|---|---|---|---|
| Step | 1 | 2 | 3 | 4 |
| Δ Temp (°C) | 500 | 100 | 50 | 25 |
| Temp (°C) | 500 | 560 | 585 | 600 |
| Dwell Time (h) | 0.1 | 0.1 | 0.1 | 24 |

| Boehmite (Catalpa A) to δ-Al$_2$O$_3$ | | | | | | |
|---|---|---|---|---|---|---|
| Step | 1 | 2 | 3 | 4 | 5 | 6 |
| Δ Temp (°C) | 600 | 100 | 100 | 50 | 25 | 25 |
| Temp (°C) | 700 | 750 | 800 | 825 | 840 | 850 |
| Dwell Time (h) | 0.1 | 0.1 | 0.1 | 0.1 | 0.1 | 24 |

**Figure 16: Oxygen Edge**



**Oxygen Edge**
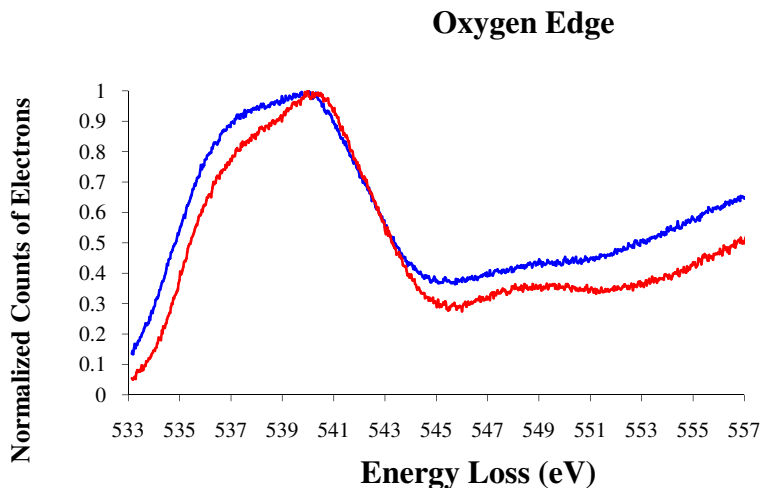
In this figure, the blue line represents $\chi$-Al$_2$O$_3$ and the red line represents $\kappa$-Al$_2$O$_3$

The first peak seems to have two prominent points in both samples, a lower one at 537 eV and a larger one at 540 eV. There seems to be a subtle difference in the height

of these two peaks between the two samples, the $\chi$ phase seeming to be at 90% of maximum peak height at 537 eV while the $\kappa$ phase is only at 80% of maximum peak height at this point. The broad peak around 547 eV in the $\kappa$ phase seems much more pronounced than the one at a similar point in the $\chi$ phase. However, these results are quite subtle, and replication is required to verify this data. Such satisfactorily replication was not carried out for the reasons discussed above.

In addition to this fragmentary data, it may be valuable to replicate portions of this experiment, especially taking a different approach to phase confirmation, in order to solidify the results of this study. There are also at least two more transition phases of $Al_2O_3$ that I have not examined for an EELS fingerprint: the $\eta$ and $\rho$ phases obtained along the path of annealing bayerite to corundum. Extensive study of the $\rho$ phase is not yet feasible with current technology, and results would likely not be applicable in the industrial world. It is extremely reactive and must be kept under high vacuum, reacting on contact with water vapor to form gibbsite or boehmite [4].

# Bibliography

[1]        C.R. Hammond, in *CRC Handbook of Chemistry and Physics, Internet Version 2007, (87th Edition), <http://www.hbcpnetbase.com>*, edited by D.R. Lide (Taylor and Francis, Boca Raton, FL, 2007).

[2]        D. Cullen and R. Vanfleet, *Fingerprinting the α and γ phases of alumina using electron energy-loss spectroscopy*, Brigham Young University Capstone Project (Unpublished).

[3]        K. Wefers and C. Misra, Oxides *and Hydroxides of Aluminum* (Alcoa Laboratories, 1987).

[4]        P. Santos, H. Santos, and S.P. Toledo, Mat. Res. [online], 3 (4), 104-114 (2000) <http://www.scielo.br/scielo.php?script=sci_arttext&pid=S1516-14392000000 400003&lng=es&nrm=iso>.

[5]        V.Y. Gertsman and Q.S.M. Kwok, Microsc. Microanal. 11, 410-420 (2005).

[6]        I. Levin and D. Brandon, J. Am. Ceram. Soc., 81 [8] 1995-2012 (1998).

[7]        R. Vanfleet, personal correspondence, September 2006.

[8]        C.C. Ahn and O.L. Kirvanek (Jan 1983) *EELS Atlas, a reverence guide of electron energy loss spectra covering all stable elements*

[9]        A. Larsson, J. Zackrisson, M. Halvarsson, and S. Ruppi (2000) *EELS investigation of CVD: α-Al$_2$O$_3$, κ-Al$_2$O$_3$, and γ-Al$_2$O$_3$ coatings*.

[10]       Hillier and Baker, J. Appl. Phys. (1944) 15, 663.

[11]       Company Name:        Nabaltec AG
           Physical Address:    Alustraße 50 - 52
                                92421 Schwandorf
                                Germany
           Web Address:         http://www.nabaltec.de
           Telephone:           +49 9431 53-0
           Email Address:       info@nabaltec.de

[12]       D. Bouchet and C. Colliex, Ultramicroscopy 96 (2003) 139-152.

# Appendix A: d-spacings from EDS for the Phases of Al$_2$O$_3$ [4]

**Chi**

| d Å | I/I$_1$ | hkl |
|---|---|---|
| 2.40 | 40 | 311 |
| 2.27 | 20 | 222 |
| 2.11 | 30 | 321 |
| 1.98 | 20 | 400 |
| 1.53 | 10 | 311,333 |
| 1.39 | 100 | 440 |

**Eta**

| d Å | I/I$_1$ | hkl |
|---|---|---|
| 4.6 | 40 | 111 |
| 2.8 | 20 | 220 |
| 2.40 | 60 | 311 |
| 2.27 | 30 | 222 |
| 1.97 | 80 | 400 |
| 1.52 | 20 | 333 |
| 1.40 | 100 | 440 |
| 1.21 | 10 | 533 |
| 1.14 | 20 | 444 |
| 1.03 | 10 | 553 |

**Gamma**

| d Å | I/I$_1$ | hkl |
|---|---|---|
| 4.56 | 40 | 111 |
| 2.80 | 20 | 220 |
| 2.39 | 80 | 311 |
| 2.28 | 50 | 222 |
| 1.997 | 100 | 400 |
| 1.520 | 30 | 511 |
| 1.395 | 100 | 440 |
| 1.140 | 20 | 444 |
| 1.027 | 10 | 731 |
| 0.989 | 10 | 800 |
| .884 | 10 | 840 |
| .806 | 20 | 844 |

**Kappa**

| d Å | I/I$_1$ |
|---|---|
| 6.2 | 30 |
| 4.5 | 20 |
| 4.2 | 10 |
| 3.04 | 40 |
| 2.79 | 60 |
| 2.70 | 20 |
| 2.57 | 80 |
| 2.41 | 30 |
| 2.32 | 40 |
| 2.26 | 10 |
| 2.16 | 10 |
| 2.11 | 80 |
| 2.06 | 30 |
| 1.99 | 40 |
| 1.95 | 20 |
| 1.87 | 40 |
| 1.82 | 30 |
| 1.74 | 20 |
| 1.64 | 60 |
| 1.54 | 10 |
| 1.49 | 30 |
| 1.45 | 30 |
| 1.43 | 80 |
| 1.39 | 100 |
| 1.34 | 30 |
| 1.12 | 10 |
| 1.06 | 10 |
| 1.04 | 5 |
| 1.02 | 5 |
| 1.01 | 40 |
| 0.994 | 20 |

**Theta**

| d Å | I/I$_1$ | hkl |
|---|---|---|
| 5.70 | 2 | 200 |
| 5.45 | 10 | 001 |
| 4.54 | 18 | 201 |
| 2.837 | 80 | 400,401 |
| 2.730 | 65 | 202,002 |
| 2.566 | 14 | 111 |
| 2.444 | 60 | 111 |
| 2.315 | 45 | 401,310 |
| 2.257 | 35 | 402,202 |
| 2.019 | 45 | 311,112 |
| 1.9544 | 8 | 601 |
| 1.9094 | 30 | 600,312 |
| 1.7998 | 14 | 510 |
| 1.7765 | 6 | 602,402 |
| 1.7376 | 4 | 403 |
| 1.6807 | 2 | 601 |
| 1.6216 | 6 | 203,511 |
| 1.5715 | 2 | 113 |
| 1.5426 | 60 | 313 |
| 1.5120 | 6 | 603 |
| 1.4883 | 25 | 113,801 |
| 1.4526 | 25 | 020 |
| 1.4264 | 10 | 800,710 |
| 1.3883 | 100 | 712,512 |

**Delta**

| d Å | I/I$_1$ | hkl |
|---|---|---|
| 7.6 | 4 | 101 |
| 6.4 | 4 | 102,004 |
| 5.53 | 4 | 111 |
| 5.10 | 8 | 112 |
| 4.57 | 12 | 113 |
| 4.07 | 12 | 114,105 |
| 3.61 | 4 | 115 |
| 3.23 | 4 | 116 |
| 3.05 | 4 | 107,214 |
| 2.881 | 8 | 117 |
| 2.728 | 30 | 222 |
| 2.601 | 25 | 302,118 |
| 2.460 | 60 | 312 |
| 2.402 | 16 | 313 |
| 2.315 | 8 | 314,305 |
| 2.279 | 40 | 226 |
| 2.160 | 4 | 1.1.10 |
| 1.986 | 75 | 400 |
| 1.953 | 40 | 0.0.12 |
| 1.914 | 12 | 318 |
| 1.827 | 4 | 319,2.2.10 |
| 1.810 | 8 | 426,3.1.11 |
| 1.628 | 8 | 1.1.14 |
| 1.604 | 4 | 513 |
| 1.538 | 8 | 1.1.15 |
| 1.517 | 16 | 523,516 |
| 1.456 | 8 | 440 |
| 1.407 | 50 | 4.0.12 |
| 1.396 | 100 | |

**Corundum α-Al$_2$O$_3$**

| d Å | I/I$_1$ | hkl |
|---|---|---|
| 3.479 | 75 | 012 |
| 2.552 | 90 | 104 |
| 2.379 | 40 | 110 |
| 2.165 | <1 | 006 |
| 2.085 | 100 | 113 |
| 1.964 | 1 | 202 |
| 1.740 | 45 | 024 |
| 1.601 | 80 | 116 |
| 1.546 | 3 | 211 |
| 1.514 | 5 | 122 |
| 1.510 | 7 | 018 |
| 1.404 | 30 | 124 |
| 1.374 | 50 | 030 |
| 1.337 | 1 | 125 |
| 1.276 | 3 | 208 |
| 1.293 | 15 | 1.0.10 |
| 1.2343 | 7 | 119 |
| 1.1898 | 7 | 220 |
| 1.1600 | <1 | 306 |
| 1.1470 | 5 | 223 |
| 1.1382 | 1 | 311 |
| 1.1255 | 5 | 312 |
| 1.1246 | 3 | 128 |
| 1.0988 | 7 | 0.2.10 |
| 1.0831 | 3 | 0.0.12 |
| 1.0781 | 7 | 134 |
| 1.0426 | 13 | 226 |
| 1.0175 | 1 | 402 |
| 0.9976 | 11 | 1.2.10 |
| 0.9857 | | 1.1.12 |
| 0.9819 | 3 | 404 |
| 0.9431 | <1 | 321 |
| 0.9413 | <1 | 1.2.11 |
| 0.9345 | 3 | 318 |
| 0.9178 | 3 | 229 |
| 0.9076 | 13 | 324 |
| 0.9052 | 3 | 0.1.14 |
| 0.8991 | 7 | 410 |
| 0.8884 | <1 | 235 |

# Appendix B: Diffraction Data

Enclosed is a CD containing 270 pages of diffraction data. The first row of data contains the d-spacings for each phase in question. The first column contains all of the d-spacings obtained from several diffraction patterns, organized by phase from largest spacing to smallest spacing.

At each intersection of row and column is a number indicating the percent difference of the experimental d-spacing from the theoretical d-spacings. The entries that have red numbers are those that are within 2% of the theoretical d-spacings to show those values that possibly correspond.

As stated earlier, it is difficult from this data to draw any concrete conclusions; nevertheless, it is presented here as part of this project's work.